Published in final edited form as:
Nat Chem Biol. 2019 March ; 15(3): 241–249. doi:10.1038/s41589-018-0211-4.

Bacterial sensors define intracellular free energies for correct enzyme metalation

Deenah Osman[#1,2], **Maria Alessandra Martini**[#1], **Andrew W. Foster**[#1,2], **Junjun Chen**[3], **Andrew J. P. Scott**[1], **Richard J. Morton**[4], **Jonathan W. Steed**[2], **Elena Lurie-Luke**[1], **Thomas G. Huggins**[3], **Andrew D. Lawrence**[5], **Evelyne Deery**[5], **Martin J. Warren**[5], **Peter T. Chivers**[1,2], and **Nigel J. Robinson**[1,2,*]

[1]Department of Biosciences, Durham University, Durham, UK

[2]Department of Chemistry, Durham University, Durham, UK

[3]Procter and Gamble, Mason Business Center, Cincinnati, Ohio, USA

[4]Department of Mathematics, Physics and Electrical Engineering, Northumbria University, Newcastle-upon-Tyne, UK

[5]School of Biosciences, University of Kent, Canterbury, Kent, UK

[#] These authors contributed equally to this work.

Abstract

There is a challenge for metalloenzymes to acquire their correct metals because some inorganic elements form more stable complexes with proteins than do others. These preferences can be overcome provided some metals are more available than others. However, while the total amount of cellular metal can be readily measured, the available levels of each metal have been more difficult to define. Metal-sensing transcriptional regulators are tuned to the intracellular availabilities of their cognate ions. Here we have determined the standard free energy for metal

[*]Correspondence and requests for materials should be addressed to N.J.R. (nigel.robinson@durham.ac.uk), or P.T.C. (peter.chivers@durham.ac.uk).

Data availability
All source data are available within the article and its Supplementary Information files, or from the corresponding author upon request. Correspondence and requests for materials should be addressed to nigel.robinson@durham.ac.uk.

Code availability
Equation derivations, template Excel spreadsheet (with instructions) and MATLAB codes (with instructions) are available in Supplementary Note 2, Supplementary Dataset and Supplementary Note 3, respectively.

Author Contributions D.O. conducted the *in vivo* experiments, bioinformatics analyses and was involved in all *in vitro* measurements of sensor affinities. M.A.M. determined *in vitro* affinities of MntR and Fur. M.A.M., along with D.O., A.W.F. and J.W.S., developed computational methods to determine θ_D and θ_{DM}. R.J.M. along with D.O. generated the MATLAB code relating fractional sensor responses to buffered [metal]. A.J.P.S and P.T.C determined the *in vitro* affinities of NikR. J.C. and T.G.H. performed the MRM tandem mass spectrometry. A.W.F. along with E.D., A.D.L., P.T.C. and M.J.W. performed and co-designed analyses of CbiK. N.J.R. and E.L.-L. conceived the programme. N.J.R., D.O. and A.W.F. drafted the manuscript and, in conjunction with M.A.M., interpreted the significance of the data. N.J.R., with input from P.T.C., had overall responsibility for the design, coordination and management of the project. All authors reviewed the results and edited and approved the final version of the manuscript.

Competing Financial Interests Statement. J.C. and T.G.H. are employees of Procter and Gamble. The collaboration was supported by an Industrial Partnership Award from the BBSRC plus a financial contribution from Procter and Gamble (in association with BBSRC award BB/J017787/1).

Europe PMC Funders Author Manuscripts

complex formation to which each sensor, in a set of bacterial metal sensors, is attuned: The less competitive the metal, the less favorable the free energy and hence greater availability to which the cognate allosteric mechanism is tuned. Comparing these free energies with values derived from the metal affinities of a metalloprotein reveals the mechanism of correct metalation exemplified here by a cobalt-chelatase for vitamin B_{12}.

Metalloenzymes catalyse approximately half of the reactions of life1–4. However, because proteins are flexible, they select metals imperfectly and have a common order of affinities with, for example, copper and Zn(II) forming tighter complexes than Mn(II)1–4. This raises a question about how cells simultaneously metalate proteins that require tight-binding metals and those that require more weakly binding ones. A solution is for cells to maintain more competitive metals at lower availabilities than less competitive ones2. Under these conditions, subtle differences in metal affinities between proteins should enable them to acquire different metals, but what are the vital metal availabilities and how can they be measured?

Bacterial DNA-binding, metal-sensing transcriptional regulators control the expression of genes encoding proteins involved in metal homeostasis, including transport proteins that import metals which are deficient or export those in excess5–7. Sensitivity is tuned to a buffered, available, intracellular metal concentration, such that when sensitivity is adjusted, a sensor ceases to detect any change in metal levels8. The metal affinities of sensors (K_1, Fig. 1a), have previously been used as first approximations of their metal sensitivities, and such values suggest that Cu(I) and Zn(II) are indeed held to lower availabilities than Mn(II)5,6,9. Furthermore, various types of estimates of intracellular metal concentrations from diverse organisms support a view that the cytosol buffers metals that form more stable complexes to lower concentrations than those that form weaker complexes8. For example, fluorescent probes indicate that cytosolic Cu(I) and Zn(II) are at much lower available concentrations than Mn(II)10. By further developing an approach that accounts for allostery as well as K_1, which was used to determine the metal sensitivities and specificities of Co(II) and Zn(II) sensors in *Salmonella* Typhimurium (hereafter *Salmonella*)11, the purpose of this work was to measure the sensitivities of a complete set of metal sensors in order to define metal availabilities inside a cell and, by so doing, to understand the mechanism of protein metalation.

In the course of this work, seven sensors were further characterised in *Salmonella*. For each sensor, the objective was to calculate change in DNA binding (or activation of the two activators) as a function of available intracellular metal concentration. To do this, a complete set of parameters have been measured and combined. At each buffered metal concentration, a fraction of each DNA target will be bound to its cognate sensor (θ_D). For the two activators, the proportion bound solely to metalated sensor is the relevant parameter (θ_{DM}), since only the metal-bound forms of these activators distort the respective promoters to enable the recruitment of RNA polymerase (Fig. 1b)12. Since metal and DNA binding are allosterically coupled, it should be possible to calculate these fractions (θ_D or θ_{DM}) if the number of sensor molecules per cell (P), the number of promoter targets per cell (D), the affinity of each sensor for its cognate metal (K_1), the affinity for DNA of metal-free and of

metal-bound sensor (K_3 and K_4 respectively in Fig. 1a) are all known11. Importantly, metal transfer between the sensors and exchangeable intracellular binding sites (metal buffer), can occur by associative ligand exchange (K_6 to K_9 in Fig. 1a), even when the intracellular milieu buffers a metal to a concentration equating to less than one hydrated ion per cell volume ($<2 \times 10^{-9}$ M for *Salmonella*). Ligand exchange reactions can be rapid, enabling thermodynamic equilibrium to be approached without (slow) metal release to the hydrated state. Here, we have obtained the above thermodynamic values for the set of *Salmonella* metal sensors. All of these parameters were then combined, taking into account any change in sensor abundance with exposure to metal, in order to calculate θ_D or θ_{DM} as a function of metal concentration and hence the tuning of each sensor.

The purpose of this work was to understand the mechanism by which proteins acquire the correct metal. The cobalt chelatase for vitamin B_{12} biosynthesis was used as an exemplar and its affinities for metals determined. In isolation, these affinities suggested that the chelatase should become mis-metalated with copper. But, when values for the chelatase were compared to the buffered intracellular metal availabilities to which the sensors were attuned, the mechanism of correct metalation with cobalt was revealed.

Results

The metals detected by *Salmonella* sensors

There is experimental evidence that six DNA-binding proteins regulate gene expression in a metal-dependent fashion in *Salmonella*11,13,14: These DNA-binding proteins include two metal-dependent transcriptional activators (the copper efflux regulator CueR and the zinc transcriptional regulator ZntR15), a metal-dependent de-repressor (the resistance to cobalt and nickel regulator RcnR16,17), and metal-dependent co-repressors (the manganese transport regulator MntR18, the ferric uptake regulator Fur and the zinc uptake regulator Zur19–21). One additional metal-dependent co-repressor (the nickel-responsive regulator NikR) can also be predicted from homology and was therefore included in this study (Supplementary Fig. 1)22. Consensus nucleotide-binding sequences have been identified in the promoters of genes regulated by each sensor (Supplementary Fig. 1b,c). The cognate metals detected by each *Salmonella* sensor were first authenticated by measuring the expression of their target genes by quantitative PCR (qPCR; Fig. 1c) and end-point reverse transcriptase PCR after prolonged (4 to 16 h) exposure of cultures to metal concentrations that inhibit growth by ≤15% (Supplementary Fig. 2). Transcripts under the control of activators CueR and ZntR increased in abundance in response to Cu(I) and Zn(II) respectively, those controlled by de-repressor RcnR increased in response to Co(II) and Ni(II), while those controlled by co-repressors MntR, Fur, Zur, and NikR decreased in abundance in response to Mn(II), Fe(II), Zn(II) and Ni(II) respectively (Fig. 1c and Supplementary Fig. 2d-g).

Affinities of sensors that complete a set of values

Metal and DNA affinities have recently been measured for RcnR and Zur11, and a Cu(I) affinity was previously determined for CueR23. To enable unknown affinities to be measured, six *Salmonella* sensors were over-expressed and purified to homogeneity (Fig.

1d), including Zur for additional measurements of non-specific DNA binding and the effect of salt on DNA binding affinity. One monomer-equivalent of Ni(II) (Fig. 2a), two monomer-equivalents of Fe(II) (Fig. 2b), and two monomer-equivalents of Mn(II) (Fig. 2c), co-migrated with NikR, Fur and MntR, respectively, during gel-filtration chromatography. Upon titration of NikR (10.6 μM) with Ni(II), a Ni(II)-NikR absorbance feature at 302 nm increased linearly and saturated at ~ 10 μM Ni(II), again indicating a stoichiometry of 1:1 Ni(II):NikR (Fig. 2d,e). Competition between NikR and EGTA for Ni(II) enabled calculation of a Ni(II) affinity (Fig. 2f, Table 1). Upon titration of Fur (10.3 μM) with Fe(II), fluorescence decreased linearly and saturated at ~ 20 μM Fe(II), consistent with a stoichiometry of 2:1 Fe(II):Fur (Fig. 2g,h). Competition between Fur and nitrilotriacetic acid (*NTA*) for Fe(II) enabled determination of a Fe(II) affinity (Fig. 2i, Table 1). The affinity of MntR for Mn(II) was determined by competition with the fluorescent probe mag-fura-2 (Fig. 2j), and a Mn(II)-affinity (6.1 (±0.4) × 10^{-6} M) for mag-fura-2 was separately established by direct titration (Fig. 2k). These data showed that Mn(II) has the weakest affinity for its cognate sensor, relative to other metals and cognate sensors (Table 1).

Binding of five sensors to DNA was monitored by fluorescence anisotropy with hexachlorofluorescein-labelled promoter fragments at limiting concentrations (Supplementary Fig. 6). The numbers of multimers (dimer or tetramer) that formed the tightest DNA complexes were also analysed with high (>0.1 μM) concentrations of DNA (Supplementary Fig. 7). DNA-binding affinities, K_3 and K_4, were then determined (Table 1). Metalated co-repressors (NikR, Fur and MntR) (Supplementary Fig. 6f–h) formed tighter DNA complexes than their metal-free forms (Supplementary Fig. 6a–c), supporting their mechanism.

Metals change the abundance of two sensors

Some sensors are auto-regulatory, and this variable has not previously been taken into account in determinations of metal sensitivity. The copy number (active multimers) per cell of each of the seven sensors was next determined by quantitative multiple reaction monitoring (MRM) mass spectrometry using cells cultured in the presence and absence of elevated concentrations of cognate metal, P_1 and P_0 respectively (Fig. 3a,b and Supplementary Fig. 8). The data showed that the abundances of the Fe(II) and Co(II) sensors changed substantially in response to metal. In low iron, cells contained approximately ten times more Fur dimers than any other sensor, consistent with its large regulon, and this number more than doubled in elevated iron (Fig. 3b). Similarly, RcnR increased by four-fold in elevated Co(II).

We recently developed a method to simultaneously solve the equilibria in Figure 1a and calculate θ_D or θ_{DM}, as shown in Figure 1b, at different intracellular buffered Co(II) and Zn(II) concentrations, but this did not account for change in sensor abundance with metal11. For co-repressor Fur, this method was used to calculate promoter occupancy (θ_D) at different concentrations of Fe(II) in cells with fixed sensor abundances P_0, P_1, and at protein abundance intervals of 10% (Fig. 3c). These data show that occupancy of some Fur-sites require *de novo* synthesis of Fur in elevated iron (~15%: The difference between the maximum values with P_0 and P_1 on Fig. 3c). If the affinity of *Salmonella* Fe(II)-Fur for its

DNA sites shows some variation, then the weaker sites will only become occupied as the amount of Fur increases in iron, contributing towards a graded response to iron at different Fur-regulated promoters24. By relating change in sensor abundance to change in promoter occupancy (Fig. 3c), further equations were derived to incorporate metal-dependent changes in sensor abundance (Supplementary Note 2, Supplementary Dataset). Applying these equations revealed hysteresis modulating sensitivity to Co(II) and Fe(II) (Fig. 3c,d). De-repression by Co(II)-RcnR of its own promoter leads to more RcnR being produced: In turn, increased RcnR suppresses the magnitude of de-repression and so the response calculated with the metal-dependent change of RcnR abundance P_T is attenuated at lower [Co(II)] relative to a model with P_0 alone (Fig. 3d).

Low buffered cytosolic metal relative to metal cell^{-1}

By applying the equations in Supplementary Note 2, via the spreadsheet in Supplementary Dataset, the response of every sensor (θ_D or θ_{DM}) to intracellular buffered concentrations of their cognate metal (K_5) was next calculated from the K_1, K_2 and K_3 values in Table 1, P_0 and P_1 values in Supplementary Figure 8b, and number of DNA targets in Supplementary Table 1 (Fig. 4a). The analyses assume that the total amount of buffer and metal are sufficiently high that binding of metal to the sensor has no substantial effect on the buffered pool of metal. Simulations using solely metal affinity K_1 matched the sensitivity for only two of the sensors, and the remainder differed by approximately an order of magnitude, some higher and others lower (Supplementary Fig. 10). Although these differences appeared relatively small on scales spanning eighteen log units, they were sufficient to influence subsequent predictions of metal specificities of the cobalt chelatase CbiK. Protein DNA affinities follow a double-log dependence on salt concentration25,26, as shown for Zur and NikR (Supplementary Fig. 11). At 500 mM K^+ plus Na^+(400 mM plus 100 mM respectively), metal sensitivities of most sensors move closer to predictions obtained using solely K_1 (Supplementary Fig. 12). The experimental conditions used here, 300 mM K^+ plus Na^+, were chosen to reflect standard internal ion concentrations. Non-halophilic bacteria such as *Salmonella* and *E. coli* maintain a relatively constant intracellular K^+ concentration within the range 200 to 500 mM27,28, with 240 mM K^+ used here, and in standard M9 medium (containing 42 mM Na^+) internal Na^+ is in the region of 50 mM27, with 60 mM Na^+ used here.

Does a consideration of sensor-binding to non-specific DNA alter predicted metal sensitivities? The amount of competing non-specific DNA per *E. coli* cell is estimated to be 10^{-4} M base pairs, with the remainder occluded, for example by other DNA binding proteins29. Non-specific binding to the *nixA* promoter was analysed for Zn(II)-Zur and apo-Zur, then estimated for the other sensors, allowing cubic equations that account for competition from non-specific DNA to be solved (Supplementary Fig. 13). However, the effect of including non-specific DNA binding on metal sensitivity was negligible (Supplementary Fig. 13c). MntR was estimated to have the tightest non-specific DNA affinity (due to its relatively tight K_3) which was confirmed experimentally (Supplementary Fig. 13d).

Available metal concentrations when each cognate sensor undergoes half of its response (Fig. 4a, Supplementary Table 2), are many orders of magnitude lower than total cellular metal expressed as a concentration (Supplementary Table 3), and mostly imply negligible free, fully-hydrated, metals. The apparent total metal concentrations in metal-replete cells are within two orders of magnitude of each other for all metals. In contrast, the buffered available cytosolic metal concentrations to which sensors are attuned vary by fifteen orders of magnitude (Supplementary Table 2 and Fig. 4a): The differences between apparent total metal concentrations and available metal concentrations reflect metal in the buffer, metal that is kinetically trapped and metal that is in non-cytosolic locations.

The calculations developed here can be used to better understand graded responses in bacterial metal homeostasis and the relationship between buffered metal concentrations and total metal concentrations. A graded response to decreasing Zn(II) has been described for Zur-regulated promoters in *B. subtilis* and *E. coli*30,31. The gradation has been attributed to negative cooperativity between the Zn(II) sites of *B. subtilis* Zur, differing in affinity by ~ 20-fold31,32. Both Zn(II) sites must be occupied for tight binding to the *znuA* promoter, but only the first site is needed for the *rpsNB* promoter, which encodes an alternative ribosomal protein that does not require Zn(II) and is part of a Zn(II)-sparing mechanism when cytosolic Zn(II) pools are depleted33. By applying the calculations developed here, the sensitivity of *B. subtilis* Zur on the *znuA* promoter is remarkably similar to *Salmonella* Zur on *znuA*, while regulation of *rpsN* is approximately an order of magnitude more sensitive to intracellular Zn(II) (Supplementary Fig. 14). The greater sensitivity of Zur on the *rpsN* promoter is consistent with a role for the product of *rpsN* in 'fail-safe' ribosome synthesis upon Zn(II) depletion31. Similarly, by using the calculations developed here to re-examine regulation by *E. coli* Zur, the magnitudes of the differences in Zur responses on *znu* and on a gene encoding a ribosomal protein are estimated to be similar in *E. coli* and in *B. subtilis* (Supplementary Fig. 14). In both bacteria, the Zn(II)-sparing, ribosome-switching mechanisms respond at least an order of magnitude below the buffered Zn(II) concentration that regulates the *znu* promoters, albeit by varying K_1 in *B. subtilis* and K_4 in *E. coli* (Supplementary Fig. 14).

In Fig. 4b, a Zn(II) buffer has been simulated by assigning an affinity mid-way between proteins with 50% saturation when the responses of *Salmonella* ZntR and Zur are at 0.5 (Fig. 4a), and the buffer has been assigned a capacity to bind up to a half of the total Zn(II) found in Zn(II) supplemented cells (Supplementary Table 3). The curve thus relates change in available buffered metal concentration to total Zn(II), as the buffer transitions from depleted to saturated. The data points reflect the Zn(II) concentrations at the mid-points of the response curves for *Salmonella* ZntR and Zur (on *znuA*) plus *B. subtilis* Zur on the *rpsNB* promoter. This illustrates that while the magnitude of the differences in buffered Zn(II) concentrations that regulate *Salmonella* ZntR and Zur, plus *B. subtilis* Zur on the *rpsNB* promoter (Fig. 4b), are modest compared to variation between sensors for different metals (Fig. 4a), they become substantial when related to fractional saturation of a cytosolic Zn(II) buffer and hence total Zn(II) $cell^{-1}$.

Metal sensing follows the Irving-Williams series

The term ‘available intracellular metal concentrations’ has the potential to be misleading because many metals are buffered to less than one hydrated ion per cell (Fig. 4a, Supplementary Table 2). Crucially, the hydrated species is less relevant if metal transfer is associative (Fig. 1a). An alternative is to describe availabilities in terms of standard free energies ($\Delta G°$). By comparing standard free energies, metal partitioning can be explained without reference to metal concentrations. The affinity of an unknown protein (or other molecule: K_A), that would have 50% metal occupancy *in vivo* was therefore calculated from available metal concentrations as derived from the tuning of metal sensors, here at 0.5 of their respective responses (Supplementary Note 3, Supplementary Table 2). The $\Delta G°$ associated with metal binding to such a protein is shown, along with values for proteins with 20% and 80% occupancy (Fig. 4c). The data presented in Figure 4c reveal that the metal availabilities to which the set of metal sensors are attuned follows an order which is the inverse of the Irving-Williams series (Supplementary Fig. 15)4: The tighter the stability constants in the series, the more favorable the free energies to which the cognate allosteric mechanisms are tuned and hence the lower the metal availabilities. By also converting the metal affinities of proteins or other biomolecules to $\Delta G°$ values, a comparison of $\Delta G°$ values will predict whether or not any given metal can transfer from the buffer to the molecule, with metals flowing to the molecule with the more favorable $\Delta G°$. A comparison of $\Delta G°$ values will similarly identify metals that will be released to the cytosol from antimicrobial ionophores34.

Free energies explain metalation of B_{12} chelatase CbiK

A third of metalloenzymes acquire metals from delivery proteins and/or contain metal cofactors that have metal-delivery proteins35. To test whether the values in Figure 4c can explain how the correct metals partition to a metal-delivery pathway, the metal affinities, and hence free energies for metalation, $\Delta G°$, were determined for the CbiK cobalt chelatase from *Salmonella*. CbiK inserts cobalt in the anaerobic vitamin B_{12} biosynthesis pathway36,37. CbiK was overexpressed and purified to homogeneity (Fig. 5a). One monomer-equivalent of Co(II) co-migrated with CbiK during gel-filtration chromatography (Fig. 5b, Supplementary Fig. 16). Competition between CbiK and the fluorescent probe fura-2 for Co(II) enabled a Co(II) affinity to be calculated (Fig. 5c, Supplementary Table 4). Competition between CbiK and mag-fura-2 for Mn(II), Fe(II), Ni(II) and Zn(II) enabled affinities to be determined for Fe(II), Ni(II) and Zn(II); for Fe(II), this was done in conjunction with an Fe(II) affinity for mag-fura-2 ($5.3\ (\pm 0.65) \times 10^{-6}$ M) that was established separately (Fig. 5d–g, Supplementary Fig. 17, 18 and Supplementary Table 4). CbiK did not show any competition for Mn(II), while an affinity weaker than 20 μM was established from the co-migration of sub-stoichiometric amounts of Mn(II) with CbiK in gel filtration chromatography when the buffer contained 20 μM Mn(II), and no associated Mn(II) when the buffer was free of Mn(II) (Supplementary Fig. 16c,d). A mean (±s.d.) Cu(I) affinity of $7.7\ (\pm 1.3) \times 10^{-14}$ M for CbiK was determined by competition with bicinchoninic acid titrated up to one equivalent of Cu(I), noting that protein precipitation occurred at greater stoichiometries (Fig. 5h). Cu(I) forms the most stable complexes with CbiK in comparison to all other metals including Co(II) (Supplementary Table 4). The affinity for Co(II) is comparable to that for Zn(II) and slightly weaker than that for Ni(II) (Supplementary Table 4). Viewed in isolation, these

values suggest that CbiK would be mis-metalated by ions other than Co(II) and preferentially Cu(I).

To understand the mechanism by which CbiK acquires the correct metal, rather than Cu(I), Ni(II) or Zn(II), affinities were converted to $\Delta G°$ values and compared to the $\Delta G°$ for metalation to which sensors are tuned (Fig. 4c). CbiK only approached the $\Delta G°$ for Co(II), estimating 15.4% occupancy (Fig. 4c, Supplementary Table 4). All other metals, including Cu(I), suggested no notable occupancy with the exception of Fe(II) with an estimated 1% occupancy (Supplementary Table 4). CbiK is known to partly complement bacterial cells missing the CysG iron chelatase for siroheme synthesis38, suggesting that CbiK can, under such circumstances, obtain some Fe(II). The Co(II)-CbiK complex was sufficiently labile that no cobalt remained bound to CbiK post-purification, and following re-metalation cobalt was lost in a single purification step (Supplementary Fig. 19), unless the purification buffers were supplemented with 20 μM cobalt (Fig. 5b). Incubation of CbiK with fura-2 plus Co(II) to give $\Delta G°$ for available Co(II) matching the intracellular value shown in Supplementary Table 2, nonetheless gave an occupancy of 15.6 %, close to the anticipated value (Supplementary Fig. 19d). It is formally possible that when vitamin B_{12} is synthesised anaerobically in *Salmonella* cells, the buffered concentration of Co(II) is elevated with RcnR at greater than 0.5 of its response. When the $\Delta G°$ for metalation was approximated solely from the metal affinities of the sensors (K_1), Co(II) ceased to be the preferred metal, switching places with Fe(II) and illustrating the importance of combining all of the parameters (Supplementary Table 4, Supplementary Fig. 20).

B_{12} metalation requires CbiK when Co(II) is buffered

The insertion of cobalt into sirohydrochlorin, which occurs in the CbiK-dependent pathway for vitamin B_{12}36,37, can be monitored from changes in intense spectral features and typically from a loss of absorbance at 376 nm (Supplementary Fig. 21a)39. Cobalt sirohydrochorin formed spontaneously in the presence of Co(II) and this reaction was accelerated by CbiK (Fig. 5i). When Co(II) was buffered to the cellular $\Delta G°$ for metalation using nitrilotriacetic acid (Fig. 4c, Supplementary Table 2), the formation of cobalt sirohydrochlorin only occurred in the presence of CbiK (Fig. 5i). The comparison of $\Delta G°$ values estimated partial metalation of CbiK with Co(II) under these conditions (Supplementary Table 4). The complete conversion of sirohydrochlorin to its cobalt form reflects subsequent catalysis and kinetic trapping of cobalt. Crucially, when Co(II) was buffered to the cellular $\Delta G°$ for metalation in the absence of CbiK, spontaneous formation of cobalt sirohydrochorin was inhibited, revealing the necessity for a chelatase that is correctly poised to acquire Co(II) from the cytosolic buffer (Fig. 5i, Supplementary Fig. 21b). Where the $\Delta G°$ gradient between buffer and protein predicts low occupancy, folding and kinetic trapping post-binding can enhance saturation, but loading is predicted to become slower and the risk of mis-metalation may be greater.

Discussion

In the course of this work, representatives of a set of metal sensors were further characterised in *Salmonella* to enable their metal sensitivities to be determined (Fig. 1c–4a,

Supplementary Fig. 6). From these sensitivities the free energies for metalation to which sensors are attuned were derived (Fig. 4c, Supplementary Table 2). Metalation *in vivo* becomes predictable from these values as shown in Figure 4c. Proteins will acquire the most competitive metal for which ΔG° is favorable relative to the buffer, exemplified here by the cobalt chelatase for vitamin B_{12}, CbiK, which in this manner is predicted to correctly acquire Co(II) rather than more tightly binding metals (Fig. 4c, Fig. 5, Supplementary Table 4). By this mechanism, cells can simultaneously metalate and use enzymes requiring uncompetitive metals at the same time as enzymes that require competitive metals.

The fraction of proteins which are under-metalated, as predicted for CbiK when RcnR is at 0.5 of its response, is currently unknown. If cells commonly synthesise larger amounts of enzymes than become metalated, then these proteins will represent a substantial fraction of the buffer. Modulation of enzyme activity through metalation status, as observed in *Streptococcus pneumoniae* where Mn(II) toxicity is mediated by hypermetalation of protein phosphatase PhpP40, also becomes possible for enzymes with ΔG° for metalation close to that of the buffer.

The stability order of metal complexes, the Irving-Williams series, is shown for first row essential metals, plus Mg(II), metals commonly required by enzymes (Supplementary Fig. 15)3,4. The notion that the availability of metals in cells will be the inverse of this series is not new3,8, but here this is finally demonstrated from the ΔG° for metalation to which sensors are attuned (Fig. 4c). The series inverts after copper, and the *Salmonella* cytosol buffers Zn(II) comparably to Ni(II).

A consequence of proteins having tighter affinities for incorrect metals is the risk of mis-metalation. To support the use of metalloenzymes in biotechnology, there is a need to determine the ΔG° for metalation in other cell types, making it possible to tune the affinities of proteins, or adjust the metal saturation of the cytosol, for optimal metalation in synthetic biology. Mis-metalation is also a feature of chronic diseases including multiple neurological disorders41–44, and there is opportunity to better understand which proteins are susceptible to mal-incorporation of which metals from equivalent ΔG° values for compartments in eukaryotes. In nutritional immunity, excess or deficiencies of metals such as Zn(II) or copper, manganese or iron, limit the growth of pathogens45–49, and there is a history of using metals, chelants and ionophores as antimicrobials50. An intriguing concept is that microbes are inherently susceptible to fluctuations in metals due to the need for precise control of relative metal availabilities in order to avoid mis-metalation, over-metalation or under-metalation40,45–47. Knowledge of the ΔG° for metalation inside cells will allow new antimicrobial compounds to be tailored to release or deplete specific metals.

Online Methods

Determination of transcript abundance

Salmonella enterica serovar Typhimurium strain SL1344 (J.S. Cavet, University of Manchester), originally from the *Salmonella* Genetic Stock Centre, was used throughout as wild-type. Media and cultures were prepared in plasticware or acid-washed glassware to minimise trace metal contamination.

For *iroB, rcnA, copA* and *zntA*, overnight cultures in M9 minimal medium, supplemented with thiamine (10 μg ml^{-1}) and L-histidine (20 μg ml^{-1}), were diluted to an $OD_{600\ nm}$ of 0.025 in fresh supplemented M9 media and cultured aerobically at 37 °C, with shaking (200 rpm), for 4-5 hours. For *znuA*, 25 μM EDTA was included to chelate basal Zn(II). For *nixA* and *mntS*, 1 × M9 salts, 0.4% w/v glucose, 10 mM sodium fumarate and 10 mM sodium formate was chelex-treated (2-3 hours) before addition of $MgSO_4$ (2 mM), $CaCl_2$ (0.1 mM), thiamine (10 μg ml^{-1}) and L-histidinol (1 mM). L-histidinol was an alternative to L-histidine minimising Ni(II)-$(L\text{-histidine})_2$ entry via NikA51. Overnight cultures were diluted to an $OD_{600\ nm}$ of 0.0001 in fresh media and cultured anaerobically for 14 - 16 h at 37 °C in capped microcentrifuge tubes without headspace.

Growth media was supplemented with metal salts as appropriate: $MnCl_2$ (200 μM), $FeSO_4$ (1 μM), $CoCl_2$ (0.5 μM), $NiSO_4$ (50 μM), $CuSO_4$ (25 μM) or $ZnSO_4$ (50 μM). Metal stocks were quantified by ICP-MS. Under aerobic conditions these concentrations cause minimal growth inhibition11,23, and inhibit growth (final cell density) by ≤15% at the point of RNA extraction (Supplementary Fig. 2a-c). Under anaerobic conditions, 5 μM $CoCl_2$ and 1 μM $CuSO_4$ inhibit growth by ≤15% at the point of RNA extraction (Supplementary Fig. 2b). RNA was extracted and cDNA generated using up to 1 μg RNA per reverse-transcriptase reaction (50 μl)11. Controls without reverse transcriptase were generated in parallel. Transcript abundance was assessed by end-point PCR and qPCR using oligonucleotide pairs 1 and 2 (*mntS*), 3 and 4 (*iroB*), 5 and 6 (*rcnA*), 7 and 8 (*nixA*), 9 and 10 (*copA*), 11 and 12 (*zntA*), 13 and 14 (z*nuA*), and 15 and 16 (*rpoD*) each designed to amplify a 100-200 bp fragment (Supplementary Table 5). End-point PCR fragments were resolved by agarose gel electrophoresis (1.5% w/v agarose) and imaged using a Gel-Doc XR+ gel documentation system. qPCR was conducted with 5 ng cDNA and three technical replicates per reaction11. The fold change, relative to the mean of the control condition for each sensor, was calculated using the $2^{-\Delta\Delta CT}$ method52, with *rpoD* as a reference. C_T values were calculated with LinRegPCR after correcting for amplicon efficiency53.

Protein expression and purification

Over-expression and purification of RcnR, CueR, ZntR and Zur has been described11,23. The *mntR*, *fur*, *nikR* and *cbiK* coding regions were amplified from *Salmonella* genomic DNA using primers 17-24 (Supplementary Table 5) and ligated into the NdeI (BfaI used to produce NdeI compatible overhang for *cbiK*) and EcoRI sites of pET29a (generating pETmntR, pETfur, pETnikR and pETcbiK, respectively). *E. coli* BL21(DE3) transformed to kanamycin (50 μg ml^{-1}) resistance with these plasmids, was cultured (37 °C, 180-200 rpm) in LB. Protein expression was induced with 1 mM IPTG (0.2 mM for pETcbiK), with addition of 50 μM $ZnSO_4$ (2-3 h).

Cells overexpressing Fur were suspended in 300 mM NaCl, 5 mM imidazole, 1 mM Tris(2-carboxyethyl)phosphine hydrochloride (TCEP), 20 mM sodium phosphate buffer pH 7.4, plus protease inhibitor cocktail (Sigma) for lysis. Following lysis and clarification, lysate was applied to 5 ml HisTrap FF (GE Healthcare) equilibrated with suspension buffer. Column was washed with suspension buffer (eight column volumes, CV), then suspension buffer containing 10 mM imidazole (2 CV), and 100 mM imidazole (0.9 CV), before elution

with suspension buffer containing 300 mM imidazole. Eluate was diluted 1 in 3 with 1 mM TCEP and 10 mM HEPES pH 7.0 before application to a 5 ml Q HP column (GE Healthcare) equilibrated with 100 mM NaCl, 1 mM TCEP, 10 mM HEPES pH 7.0, washed with equilibration buffer (5 CV) and eluted with equilibration buffer containing 1 M NaCl. Fur concentration was estimated via $A_{280\ nm}$ (determined $\varepsilon_{280\ nm}$ = 6,672 M^{-1} cm^{-1}) before gradual addition of 2 molar equivalents of $ZnSO_4$ and incubation for 1 h at room temperature (to fill the Zn(II) structural site). EDTA was added to 7.5 mM (to remove excess Zn(II)) and sample incubated overnight at 4 °C. Sample was applied to HiLoad 16/600 Superdex 75 (GE Healthcare) equilibrated in 100 mM NaCl, 0.5 mM TCEP, 10 mM HEPES pH 7.0 (chelex-treated), eluted with the same buffer. Fractions containing dimeric Fur (based on elution volume) were applied to 1 ml Q HP column (GE Healthcare) equilibrated in the same buffer, moved into an anaerobic glovebox, washed with 20 mM NaCl, 80 mM KCl, 10 mM HEPES pH 7.0 (chelex-treated, N_2-purged) (10 CV), before elution with 200 mM NaCl, 800 mM KCl, 10 mM HEPES pH 7.0 (chelex-treated, N_2-purged).

Cells overexpressing MntR were suspended in 300 mM NaCl, 10 mM imidazole, 20 mM sodium phosphate buffer pH 7.4, plus 1 mM phenylmethanesulfonyl fluoride (PMSF) for lysis. Following lysis and clarification, lysate was applied to a 5 ml HisTrap HP column (GE Healthcare) equilibrated with suspension buffer. Column was washed with suspension buffer (8 CV) before elution with suspension buffer containing 100 mM imidazole. Sample was applied to HiLoad 16/600 Superdex 75 equilibrated with 300 mM NaCl, 10 mM EDTA, 10 mM HEPES pH 7.0 and eluted with the same buffer. Pooled MntR containing fractions were loaded onto 1 ml HiTrap Heparin (GE Healthcare) equilibrated with the size exclusion buffer, washed with gel-filtration buffer (10 CV) before elution with 1 M NaCl, 10 mM EDTA, 10 mM HEPES pH 7.0. Eluate was diluted 1 in 3 with 10 mM EDTA, 10 mM HEPES pH 7.0 before application to 1 ml HiTrap Heparin equilibrated with the size exclusion buffer. Column was washed with 60 mM NaCl, 240 mM KCl, 10 mM HEPES pH 7.0 (chelex-treated) (10 CV), before elution with 200 mM NaCl, 800 mM KCl, 10 mM HEPES pH 7.0 (chelex-treated).

Cells overexpressing NikR were suspended in 500 mM NaCl, 10 mM imidazole, 100 mM sodium phosphate buffer pH 8.0. Following lysis and clarification, 100 μM $NiCl_2$ was added to the lysate which was then applied to 1.5 ml Ni(II)-NTA agarose. Column was washed with suspension buffer (15 CV) and suspension buffer containing 35 mM imidazole (10 CV) before elution with suspension buffer containing 250 mM imidazole, 100 mM NaCl. Eluate was diluted 1 in 2 with 2 mM TCEP, 10 mM HEPES pH 7.5 before application to a 5 ml Q HP column equilibrated with 100 mM NaCl, 2 mM TCEP, 10 mM HEPES pH 7.5, washed with equilibration buffer (5 CV) and eluted with equilibration buffer containing 0.5 M NaCl. EDTA (10 mM) and L-histidine (500 μM) were added (to remove Ni(II)) and sample incubated overnight at 37 °C. Sample was applied to HiLoad 16/600 Superdex 75 equilibrated in 100 mM NaCl, 1 mM TCEP, 10 mM HEPES pH 7.5 (chelex-treated) and eluted with the same buffer. Pooled NikR containing fractions were applied to 1 ml Q HP equilibrated in the same buffer and moved into an anaerobic glovebox, washed with 100 mM NaCl, 10 mM HEPES pH 7.5 (chelex-treated, N_2-purged) (10 CV), before elution with 100 mM NaCl, 400 mM KCl, 10 mM HEPES pH 7.5 (chelex-treated, N_2-purged).

Cells overexpressing CbiK were suspended in 100 mM NaCl, 1 mM DTT, 5 mM imidazole, 20 mM sodium phosphate pH 7.4 plus 1 mM PMSF for lysis. Following lysis and clarification, lysate was applied to HisTrap HP (GE Healthcare) equilibrated with suspension buffer. Column was washed with suspension buffer (10 CV), before elution with suspension buffer containing 300 mM imidazole. EDTA was added to 10 mM and sample incubated at room temperature (2 h). Sample was applied to HiLoad 26/60 Superdex 75 (GE Healthcare) equilibrated in 100 mM NaCl, 1 mM TCEP, 10 mM HEPES pH 7.0 (chelex-treated) and eluted with the same buffer. Peak elution fractions (based on SDS-PAGE analysis) were pooled and applied to 1 ml HiTrap Q HP (GE Healthcare) equilibrated in the same buffer and moved into an anaerobic glovebox. Column was washed with 20 mM NaCl, 80 mM KCl, 10 mM HEPES pH 7.0 (chelex-treated, N_2-purged) (20 CV) before elution with 40 mM NaCl, 160 mM KCl, 10 mM HEPES pH 7.0 (chelex-treated, N_2-purged). To produce semi-pure CbiK by anion exchange chromatography cells overexpressing CbiK were suspended in 100 mM NaCl, 1 mM TCEP, 10 mM HEPES pH 7.0 plus 1 mM PMSF for lysis. Following lysis and clarification, lysate was applied to 1 ml HiTrap Q HP (GE Healthcare) equilibrated with suspension buffer, column washed with suspension buffer (10 CV), before elution with suspension buffer containing 500 mM NaCl.

Protein purity was confirmed by SDS-PAGE. Fur, MntR and CbiK were quantified from $A_{280\ nm}$ and extinction coefficients obtained via quantitative amino acid analysis performed by Alta Bioscience. The extinction coefficient for denatured NikR has previously been determined (*E. coli* NikR, 99% identity)54, and was corrected for folded NikR by comparison of $A_{280\ nm}$ of folded and denatured NikR. MntR $\varepsilon_{280\ nm}$ = 7,940 M^{-1} cm^{-1}, NikR $\varepsilon_{280\ nm}$ = 4,398 M^{-1} cm^{-1}, CbiK $\varepsilon_{280\ nm}$ = 24,802 M^{-1} cm^{-1}. Thiol and metal content were assayed as previously described11, and all protein samples were ≥90% reduced (with the exception of CbiK, MntR has no thiols) and ≥95% metal-free (Fur contained ~1 molar equivalent of Zn(II)). CbiK was typically <90% reduced and none of the cysteines are proximal to the active/metal binding site55. All *in vitro* experiments were carried out under anaerobic conditions using chelex-treated and N_2-purged buffers, other than MntR (aerobic, chelex-treated buffers).

Preparation of anaerobic metal stocks

Concentrations of all metal stocks were determined by ICP-MS. $(NH_4)_2Fe(SO_4)_2.6H_2O$ was dissolved in N_2-purged 0.1% v/v HCl under anaerobic conditions and confirmed to be >90% reduced by titration into an excess (~ 10-fold) of ferrozine, 3 ferrozine: 1 Fe(II) $\varepsilon_{562\ nm}$= 27,900 M^{-1} cm^{-1} 56. Dilutions from this stock were prepared daily in N_2-purged ultrapure H_2O and confirmed to be >90% Fe(II). CuCl was prepared as described previously and confirmed to be >95% reduced by titration against bathocuproine sulfonate (BCS)57. Other metal salts were dissolved in ultrapure H_2O.

Determination of metal stoichiometries and affinities

All experiments conducted in 100 mM NaCl, 400 mM KCl, 10 mM HEPES pH 7.0, with inclusion of 5% v/v glycerol for competition of MntR with mag-fura-2 or at pH 8.0 for NikR gel-filtration chromatography and UV-Vis spectroscopy to determine Ni(II)-binding stoichiometry. Scripts for affinity determinations, for use with Dynafit58, are in

Supplementary Note 1. Gel-filtration chromatography of NikR, MntR, Fur and CbiK (all 20 μM monomer other than CbiK (10 μM monomer), 0.5 ml, recovery of NikR was routinely <100%) was performed using Sephadex G25 (GE Healthcare), with buffer supplemented with 100 μM $MnCl_2$ (MntR), 50 μM $(NH_4)_2Fe(SO_4)_2$ (Fur) and either 20 μM $CoCl_2$, $MnCl_2$ or un-supplemented (CbiK). Where required, proteins were pre-incubated for 30 min with 20 μM $MnCl_2$ (CbiK), 1.2 molar equivalents of $NiCl_2$ (NikR), 100 μM $MnCl_2$ (MntR) and either 50 μM $(NH_4)_2Fe(SO_4)_2$ or 1 mM EDTA (Fur). Fractions (0.5 ml) were analysed for metal by ICP-MS and protein by Bradford assay or $A_{280\ nm}$.

Increasing concentrations of $NiCl_2$ were added to solutions of NikR (12.8-15.6 μM) and EGTA, equilibrated overnight at room temperature. Absorbance of Ni(II)-NikR was measured using a λ35 UV-visible spectrophotometer (PerkinElmer). Data were fit to a model describing NikR competition for one molar equivalent of Ni(II) (per monomer) using Dynafit58. EGTA Ni(II)-affinity = 4.98×10^{-10} M at pH 7.0 determined using Schwarzenbach's α co-efficient.

$(NH_4)_2Fe(SO_4)_2$ was titrated into Fur solution in the absence (10-18 μM Fur; to determine Fe(II) stoichiometry), or presence (10-11 μM Fur) of nitrilotriacetic acid (NTA). Fur fluorescence emission was recorded at equilibrium (Cary Eclipse fluorescence spectrophotometer (Agilent Technologies), λ_{ex} = 276 nm, 25 °C). Data were fit to a model describing Fur competition for two molar equivalent of Fe(II) using Dynafit58, with positive cooperativity between two pairs of sites per dimer. NTA Fe(II)-affinity = 6.77×10^{-7} M at pH 7.0 determined using Schwarzenbach's α co-efficient.

$MnCl_2$ was titrated into a solution of mag-fura-2 in the absence (to determine mag-fura-2 Mn(II)-affinity) or presence of MntR (7.1-18.7 μM). Mag-fura-2 ($\varepsilon_{369\ nm}$= 22,000 M^{-1} cm^{-1} 23) fluorescence excitation was recorded at equilibrium (Cary Eclipse fluorescence spectrophotometer, λ_{em} = 505 nm, 20 °C). Data were fit to a model describing 1:1 Mn(II):mag-fura-2 stoichiometry and MntR competition for two molar equivalents of Mn(II) per monomer, using Dynafit58; mag-fura-2 $K_{Mn} = 6.1\ (\pm 0.4) \times 10^{-6}$ M.

$MnCl_2$, $(NH_4)_2Fe(SO_4)_2$, $NiCl_2$ or $ZnSO_4$ were titrated into a solution of mag-fura-2 in the presence of CbiK and absorbance (325 and 366 nm) recorded at equilibrium (λ35 UV-visible spectrophotometer). Data were fit to models describing 1:1 metal:mag-fura-2 and 1:1 metal:CbiK stoichiometry, using Dynafit58; mag-fura-2 $K_{Ni} = 5 \times 10^{-8}$ M 59, $K_{Zn} = 2 \times 10^{-8}$ M 23, and $K_{Fe} = 5.3 \times 10^{-6}$ M (determined by direct titration of mag-fura-2 with $(NH_4)_2Fe(SO_4)_2$).

$CoCl_2$ was titrated into a solution of fura-2 ($\varepsilon_{363\ nm}$= 28,000 M^{-1} cm^{-1} 23) in the presence of CbiK and fluorescence emission recorded at equilibrium (Cary Eclipse fluorescence spectrophotometer, λ_{ex} = 360 nm, 20 °C). Data were fit to a model describing 1:1 Co(II): fura-2 and 1:1 Co(II):CbiK stoichiometry, using Dynafit58; fura-2 $K_{Co} = 8.6 \times 10^{-9}$ M 23.

CuCl was titrated into a solution of bicinchoninic acid (BCA) and absorbance of Cu(I):BCA_2 ($\varepsilon_{562\ nm}$ = 7,900 M^{-1} cm^{-1} 60) recorded at equilibrium (λ35 UV-visible spectrophotometer). Precipitation at [CuCl] greater than 1:1 Cu(I):CbiK precluded data fitting so CbiK K_{Cu} was determined from individual equilibrium values using Equation 1:

$$K_D\beta_2 = \frac{\left(\frac{[P]_{total}}{[MP]}\right) - 1}{\{\left(\frac{[L]_{total}}{[ML_2]}\right) - 2\}^2 [ML_2]} \quad (1)$$

Where $[P]_{total}$ and $[L]_{total}$ are the total concentrations of CbiK and BCA, respectively, K_D is the Cu(I) dissociation constant of CbiK, β_2 is the formation constant of Cu(I):BCA_2 ($10^{17.2}$ M^{-2} 60), and [MP] and $[ML_2]$ are the equilibrium concentrations of Cu(I):CbiK and Cu(I):BCA_2 determined $\varepsilon_{562\ nm}$ and mass balance.

Determination of DNA-binding affinities by fluorescence anisotropy

Fluorescently labelled double-stranded DNA probes were generated using oligonucleotides 25 and 26 (*nixA*Pro for NikR and as a non-specific probe for Zur), 27 and 28 (*mntS*Pro for MntR), 29 and 30 (*copA*Pro for CueR), 31 and 32 (*zntA*_longPro, containing an extended sequence compared to that used previously11, for ZntR), 33 and 34 (*furbox*, containing the consensus *E. coli* Fur binding site for Fur), 39 and 40 (*mntS*Proswap, a semi-randomised variant of *mntS*Pro for MntR), and 41 and 42 (*znuA*Pro for Zur) (Supplementary Table 5). In each case one oligonucleotide was hexachlorofluorescein labelled. Complementary single-stranded oligonucleotides were annealed as described previously11. All experiments, other than with Zur and some with NikR (as noted in figure legend), were conducted in 60 mM NaCl, 240 mM KCl, 10 mM HEPES pH 7.0, with inclusion of 200 μM $MnCl_2$ for Mn(II)-MntR, 5-50 μM $(NH_4)_2Fe(SO_4)_2$ for Fe(II)-Fur, 1 mM EDTA for apo-NikR, or 5 mM EDTA for all other apo-proteins. NikR was prepared in 100 mM NaCl, 400 mM KCl, 10 mM HEPES pH 8.0 with 0.95 molar equivalents of $NiCl_2$ for Ni(II)-NikR. Zur was prepared as described previously11. All other proteins were prepared in 200 mM NaCl, 800 mM KCl, 10 mM HEPES pH 7.0, with 1.2 molar equivalents of CuCl for Cu(I)-CueR, 1.2 molar equivalents of $ZnSO_4$ for Zn(II)-ZntR, 2.2 molar equivalents $MnCl_2$ for Mn(II) -MntR, 2.2 molar equivalents of $(NH_4)_2Fe(SO_4)_2$ for Fe(II)-Fur, and 5 mM EDTA for apo-MntR and apo-Fur. Proteins were titrated against labelled DNA probes and anisotropy measured using a modified Cary Eclipse Fluorescence Spectrophotometer (Agilent Technologies), settings described previously23. For Fur, NikR, CueR, Zur and ZntR, DNA-binding affinities were determined using Dynafit58 (Supplementary Note 1). For MntR, data were fit to a 2nd degree polynomial regression and limits for DNA affinities determined at the intersection of the regression line and half the Δr_{obs} value associated with binding of a MntR dimer to *mntS*Pro. Coupling free energies (ΔG_C) were derived as previously described23.

Determination of sensor protein abundance

Generation of *E. coli* strains BW25113Δ*zntR*/Δ*zur* (lacking *zntR* and *zur*), BW25113Δ*nikR*/Δ*rcnR* (lacking *nikR* and *rcnR*), and *Salmonella* strain SL1344Δ*cueR*/Δ*golS* (lacking *cueR*) have been described previously11,14. *E. coli* strains BW25113*Δfur::kan* (lacking *fur*) and BW25113*ΔmntR::kan* (lacking *mntR*) were obtained from the Keio collection (strains JW0669 and JW0801, respectively). The kanamycin resistance cassette from BW25113*ΔmntR::kan* was removed using helper plasmid pCP20 carrying FLP recombinase

Europe PMC Funders Author Manuscripts

and *Δfur::kan* fragment was moved into strain BW25113Δ*mntR* (*kan* cassette removed) by P1 transduction. The remaining kanamycin resistance cassette was removed and genotype (Δ*mntR*/Δ*f*ur) confirmed by PCR using primers 35-38 (Supplementary Table 5). *E. coli* BW25113 strains were cultured to logarithmic phase in M9 minimal medium supplemented with thiamine (10 μg ml^{-1}), and 1 μM ferric citrate (BW25113Δ*zntR*/Δ*zur* and BW25113Δ*nikR*/Δ*rcnR*) or 100 μM $FeSO_4$ (BW25113Δ*mntR*/Δ*fur*). *Salmonella* SL1344 was grown as described for transcript abundance determination of *iroB*. Purified stocks of MntR, Fur, RcnR, NikR, CueR, Zur, and ZntR were quantified by amino acid analysis (UC Davis). Purification of recombinant RcnR, Zur and ZntR, and their quantitation in *Salmonella* cells cultured with $ZnSO_4$ (ZntR and Zur), or $CoCl_2$ (RcnR) was performed as described for quantitation in cells cultured without metal supplementation11. Quantitation of MntR, Fur, NikR and CueR (in cells with and without cognate metal supplementation) was performed as for Zur and ZntR11. Standard curve samples were prepared by dilution of purified protein stocks into cell lysates from BW25113*ΔmntR*/*Δfur* (MntR and Fur), SL1344*ΔcueR*/*ΔgolS* (CueR). Heavy isotope labelled peptides ([$^{13}C_6$,$^{15}N_4$]arginine residues; Thermo Fisher) were used as working internal standards (IS). Samples were prepared and analysed by scheduled multiple reaction monitoring (MRM) mass spectrometry, as previously described11. A quadratic $1/x^2$ weighted regression model was used to perform standard curve calibration (Supplementary Fig. 8a). The transitions monitored were: 765.4/746.2 for Zur peptide ETEPQAKPPTIYR (770.4/756.2 for IS), 550.8/601.3 for ZntR peptide LADVTPDTIR (555.8/611.3 for IS), 409.2/590.3 for RcnR peptide GAVNGLMR (414.2/600.3 for IS), 500.3/730.4 for MntR peptide LGVSQPTVAK (504.3/738.4 for IS), 426.8/482.3 for CueR peptide GLVTPPLR (431.8/492.3 for IS), 690.8/1039.5 for Fur peptide VIEFSDDSIEAR (695.8/1049.5 for IS), 937.4/1171.6 for NikR peptide GDMGDVQHFADDVIAQR (942.4/1181.6 for IS).

Mathematical calculations

Fractional occupancy of DNA targets with sensor (θ_D or θ_{DM}; Fig. 1b), as a function of metal concentration ([M]), was calculated using metal affinities (K_1), DNA affinities (K_3 and K_4), cellular abundance of each sensor (P_T), and number of DNA target(s) (D) (Table 1 and Supplementary Figs. 8b, Supplementary Table 8). P_T was calculated using determined sensor concentrations in *Salmonella* cells grown without (P_0) and with supplementation of cognate metal (P_1) (Supplementary Fig. 8b), by relating fractional change in DNA occupancy to fractional change in protein abundance (Equations 2 and 3):

$$\frac{P_T - P_0}{P_1 - P_0} = \frac{\theta_D - \theta_{D0}}{\theta_{D1} - \theta_{D0}} \quad (2)$$

$$\frac{P_T - P_0}{P_1 - P_0} = \frac{\theta_{DM} - \theta_{DM0}}{\theta_{DM1} - \theta_{DM0}} \quad (3)$$

Where θ_{D0} and θ_{D1} are DNA occupancies with sensor (θ_{DM0} and θ_{DM1} for metalated sensor) at low and high cognate metal concentrations, respectively. A cell volume of 1 fl was used to calculate cellular concentrations of P_0, P_1 and D_T from values in Table 1 and Supplementary Figs. 8b and Supplementary Table 1. Equations expressing θ_D and θ_{DM} as a function of [M], were derived (Supplementary Note 2), and a template Excel spreadsheet enables calculation of θ_D or θ_{DM} (Supplementary Dataset). DNA occupancy of each sensor was normalised for inter-comparison using the minimum and maximum DNA occupancy values.

Fractional DNA occupancy inferred from K_1 only, to generate Supplementary Fig. 10a, was calculated using Equation 4:

$$\theta_S = \frac{[M]K_1}{(1 + [M]K_1)} \quad (4)$$

Where θ_S is the fractional occupancy of sensor with metal.

Simulations in Supplementary Figs. 10, 12 and 14 were generated by changing one or more parameter(s) as specified in the figure legend.

DNA binding affinities at 500 mM salt were calculated based on apo-Zur, Zn(II)-Zur and apo-NikR data, then used to determine DNA occupancies, as described in Supplementary Note 2.

Non-specific DNA affinities for MntR, Fur, RcnR, NikR, ZntR and CueR were estimated based on determined Zur affinities for *nixA*Pro as described in Supplementary Note 2. To incorporate competition from non-specific DNA, further equations were derived (Supplementary Note 2) to calculate θ_D or θ_{DM}. In this case a Supplementary Dataset (spreadsheet) is not provided due to the complexity of the calculation. DNA occupancy of each sensor was normalised for inter-comparison using the minimum and maximum DNA occupancy values (Supplementary Fig. 13).

The buffered [M] corresponding to a normalised fractional DNA occupancy (θ_D or θ_{DM}) of 0.5 was determined for each sensor and indicates the available [M] in the *Salmonella* cytosol (MATLAB codes in Supplementary Note 3). The binding affinity (K_A) of a metalloprotein required for 20, 50 and 80% metal occupancy at these buffered [M] was calculated using Equation 5:

$$K_A = \frac{\theta_P}{[M](1 - \theta_P)} \quad (5)$$

K_A was used to calculate the standard free-energy for formation ($\Delta G°$) of the protein-metal complex using Equation 6 to generate Fig. 4c:

$$\Delta G^{\circ} = -RT\ln K_A \quad (6)$$

Where $R = 8.314 \times 10^{-3}$ KJ mol^{-1}K^{-1} and $T = 298.15$ K.

The concentration of Zn(II) ions associated with the buffer (Fig. 4b), was calculated using Equation 7:

$$[M_T] = \frac{K_5[M]^2 + [M](K_5[B_T] + 1)}{(1 + K_5[M])} \quad (7)$$

Where K_5 is the buffer Zn(II)-affinity and [B_T] is the concentration of buffering species (Supplementary Note 2). [Zn(II)] was converted to ions cell^{-1} using a cell volume of 1 fl.

Metal content of *Salmonella* cells

Salmonella SL1344 was grown as described for transcript abundance determination of *iroB*, and an aliquot used for cell enumeration on LB agar. Cell pellets (from 100 ml cultures) were washed once with 0.5 M sorbitol, 100 μM EDTA, 10 mM HEPES pH 7.8, and twice in the same buffer without EDTA (all 10 ml). Pellets were suspended in ultrapure 65% (v/v) HNO_3 (1 ml) to digest before metal analysis by ICP-MS.

Metalation of sirohydrochlorin

BL21*(DE3)plysS transformed with pETcoco-2ABCDC was cultured and overexpression induced as described previously (overnight expression at 20 °C)39. Cell pellets suspended in 100 mM NaCl, 10 mM imidazole, 20 mM Tris pH 8.0 for lysis. Following lysis and clarification, lysate was applied to 5 ml HisTrap HP (GE Healthcare) equilibrated with suspension buffer. Column was washed with suspension buffer (10 CV), then suspension buffer containing 60 mM imidazole (5 CV), before elution with suspension buffer containing 400 mM imidazole. In an anaerobic glovebox the peak (2.5 ml) elution fraction was applied to a Sephadex G25 equilibrated in anaerobic 100 mM NaCl, 50 mM Tris pH 8.0 and eluted directly into solution A using the same buffer. Solution A contained 20 mg *S*-adenosyl-L-methionine, 10 mg aminolevulinic acid and 6.5 mg nicotinamide adenine dinucleotide dissolved in 2 ml anaerobic 100 mM NaCl, 50 mM Tris pH 8.0 and adjusted to pH 8.0 with NaOH. Light excluded and left overnight. Reaction product applied to 1 ml HiTrap DEAE FF (GE Healthcare) equilibrated in anaerobic 100 mM NaCl, 20 mM Tris pH 8.0. Column washed with equilibration buffer containing 100, 200, 300 mM NaCl (10 CV each) and eluted with equilibration buffer containing 800 mM NaCl. Sirohydrochlorin quantified via $\varepsilon_{376\ nm}$ = 240,000 M^{-1} cm^{-1}.

Co(II) insertion into sirohydrochlorin was performed in anaerobic 100 mM NaCl, 400 mM KCl, 10 mM HEPES pH 7.0 (absence of metal buffer) or 50 mM HEPES pH 7.0 (presence of metal buffer). Supplementary Equations 34-38 (Supplementary Note 2) were used to define buffered [Co(II)], at a certain [NTA] and [Co(II)], with the NTA Co(II) association

constant at pH 7.0 (4.5×10^7 M^{-1}) determined using Schwarzenbach's α co-efficient. 2.8 mM NTA will buffer 300 μM Co(II) at 2.7×10^{-9} M, approximating the calculated intracellular buffered [Co(II)] (2.5×10^{-9} M). For Co(II) insertion in the absence of metal buffer 50 μM $CoCl_2$ was added to a solution of ~5 μM sirohydrochlorin in the absence or presence of 5 μM CbiK. For Co(II) insertion in the presence of metal buffer ~5 μM sirohydrochlorin with or without 5 μM CbiK was added to a solution of 2.8 mM NTA and 300 μM Co(II). Decrease in $A_{376\ nm}$ was monitored (λ35 UV-visible spectrophotometer). Under each condition reactions with enzyme run to equilibrium were used to define an extinction coefficient for Co(II)-loaded sirohydrochlorin.

CbiK metal occupancy in the cell was calculated using Equation 8:

$$\theta = \frac{[M]_{buffered}}{K_D + [M]_{buffered}} \quad (8)$$

Where θ is fractional protein occupancy with metal, K_D is CbiK metal dissociation constant and $[M]_{buffered}$ is the calculated intracellular buffered metal concentration.

Statistics and reproducibility

Sample sizes followed convention in the literature for equivalent analyses. To enable calculation of s.d. in experiments designed to derive quantitative values to be used in the simulations these assays were initially performed in triplicate or quadruplicate (where equipment allowed even numbers of samples) with additional replicates performed when the s.d. was initially high. The number of independent experiments or biologically independent samples is shown for each result.

Supplementary Material

Refer to Web version on PubMed Central for supplementary material.

Acknowledgements

This work was supported by Biotechnology and Biological Sciences Research Council awards BB/J017787/1, BB/R002118/1 and BB/L009226/1. Interactions with Industrial partners were supported by Biotechnology and Biological Sciences Research Council (BBSRC) award BB/L013711/1 plus a financial contribution from Procter and Gamble (in association with BB/J017787/1 Industrial Partnership Award). Kotryna Svedaite, Department of Biosciences, Durham University, provided technical assistance in the measurements of *in vitro* DNA affinities of ZntR and CueR. Ehmke Pohl and Colin Bain, both of Durham University Department of Chemistry, assisted with structure homology modelling and consideration of standard free energy changes, respectively. *Salmonella enterica* serovar Typhimurium strain SL1344 was provided by Jennifer S. Cavet, School of Biological Sciences, University of Manchester, Manchester, U.K. Elia Fioravanti, Mathematical Institute, University of Oxford, assisted with derivations shown in the Supplementary Note 2. All DNA sequencing was conducted by DBS genomics, Durham University.

References

1. Waldron KJ, Rutherford JC, Ford D, Robinson NJ. Metalloproteins and metal sensing. Nature. 2009; 460:823–830. [PubMed: 19675642]
2. Tottey S, et al. Protein-folding location can regulate manganese-binding versus copper- or zinc-binding. Nature. 2008; 455:1138–1142. [PubMed: 18948958]

3. Fraústo da Silva, JJR, Williams, RJP. The Biological Chemistry of the Elements: The Inorganic Chemistry of Life. Oxford University Press; Oxford: 1991.
4. Irving H, Williams RJP. Order of stability of metal complexes. Nature. 1948; 162:746–747.
5. Chandrangsu P, Rensing C, Helmann JD. Metal homeostasis and resistance in bacteria. Nat Rev Microbiol. 2017; 15:338–350. [PubMed: 28344348]
6. Reyes-Caballero H, Campanello GC, Giedroc DP. Metalloregulatory proteins: metal selectivity and allosteric switching. Biophys Chem. 2011; 156:103–114. [PubMed: 21511390]
7. Giedroc DP, Arunkumar AI. Metal sensor proteins: nature's metalloregulated allosteric switches. Dalton Trans. 2007:3107–3120. [PubMed: 17637984]
8. Foster AW, et al. A tight tunable range for Ni(II) sensing and buffering in cells. Nat Chem Biol. 2017; 13:409–414. [PubMed: 28166209]
9. Outten CE, O'Halloran TV. Femtomolar sensitivity of metalloregulatory proteins controlling zinc homeostasis. Science. 2001; 292:2488–2492. [PubMed: 11397910]
10. Carter KP, Young AM, Palmer AE. Fluorescent sensors for measuring metal ions in living systems. Chem Rev. 2014; 114:4564–4601. [PubMed: 24588137]
11. Osman D, et al. Fine control of metal concentrations is necessary for cells to discern zinc from cobalt. Nat Commun. 2017; 8
12. Ansari AZ, Chael ML, O'Halloran TV. Allosteric underwinding of DNA is a critical step in positive control of transcription by Hg-MerR. Nature. 1992; 355:87–89. [PubMed: 1731201]
13. Ikeda JS, Janakiraman A, Kehres DG, Maguire ME, Slauch JM. Transcriptional regulation of *sitABCD* of *Salmonella enterica* serovar Typhimurium by MntR and Fur. J Bacteriol. 2005; 187:912–922. [PubMed: 15659669]
14. Osman D, et al. Copper homeostasis in *Salmonella* is atypical and copper-CueP is a major periplasmic metal complex. J Biol Chem. 2010; 285:25259–25268. [PubMed: 20534583]
15. O'Halloran T, Walsh C. Metalloregulatory DNA-binding protein encoded by the *merR* gene: isolation and characterization. Science. 1987; 235:211–214. [PubMed: 3798107]
16. Iwig JS, Rowe JL, Chivers PT. Nickel homeostasis in *Escherichia coli* – the *rcnR-rcnA* efflux pathway and its linkage to NikR function. Mol Microbiol. 2006; 62:252–262. [PubMed: 16956381]
17. Iwig JS, Leitch S, Herbst RW, Maroney MJ, Chivers PT. Ni(II) and Co(II) sensing by *Escherichia coli* RcnR. J Am Chem Soc. 2008; 130:7592–7606. [PubMed: 18505253]
18. Que Q, Helmann JD. Manganese homeostasis in *Bacillus subtilis* is regulated by MntR, a bifunctional regulator related to the diphtheria toxin repressor family of proteins. Mol Microbiol. 2000; 35:1454–1468. [PubMed: 10760146]
19. Althaus EW, Outten CE, Olson KE, Cao H, O'Halloran TV. The ferric uptake regulation (Fur) repressor is a zinc metalloprotein. Biochemistry. 1999; 38:6559–6569. [PubMed: 10350474]
20. Hantke K. Regulation of ferric iron transport in *Escherichia coli* K12: isolation of a constitutive mutant. Mol Gen Genet. 1981; 182:288–292. [PubMed: 7026976]
21. Patzer SI, Hantke K. The ZnuABC high-affinity zinc uptake system and its regulator Zur in *Escherichia coli*. Mol Microbiol. 1998; 28:1199–1210. [PubMed: 9680209]
22. Schreiter ER, et al. Crystal structure of the nickel-responsive transcription factor NikR. Nat Struct Biol. 2003; 10:794–799. [PubMed: 12970756]
23. Osman D, et al. Generating a metal-responsive transcriptional regulator to test what confers metal sensing in cells. J Biol Chem. 2015; 290:19806–19822. [PubMed: 26109070]
24. Pi H, Helmann JD. Sequential induction of Fur-regulated genes in response to iron limitation in *Bacillus subtilis*. Proc Natl Acad Sci U S A. 2017; 114:12785–12790. [PubMed: 29133393]
25. Record MT Jr, Ha JH, Fisher MA. Analysis of equilibrium and kinetic measurements to determine thermodynamic origins of stability and specificity and mechanism of formation of site-specific complexes between proteins and helical DNA. Methods Enzymol. 1991; 208:291–343. [PubMed: 1779839]
26. Campanello GC, et al. Allosteric inhibition of a zinc-sensing transcriptional repressor: insights into the arsenic repressor (ArsR) family. J Mol Biol. 2013; 425:1143–1157. [PubMed: 23353829]

27. Epstein W, Schultz SG. Cation Transport in *Escherichia coli*: V. Regulation of cation content. J Gen Physiol. 1965; 49:221–234. [PubMed: 19873561]
28. Su J, Gong H, Lai J, Main A, Lu S. The potassium transporter Trk and external potassium modulate Salmonella enterica protein secretion and virulence. Infect Immun. 2009; 77:667–675. [PubMed: 19001074]
29. Stickle DF, Vossen KM, Riley DA, Fried MG. Free DNA concentration in *E. coli* estimated by an analysis of competition for DNA binding proteins. J Theor Biol. 1994; 168:1–12. [PubMed: 8022188]
30. Gilston BA, et al. Structural and mechanistic basis of zinc regulation across the *E. coli* Zur regulon. PLOS Biol. 2014; 12:e1001987. [PubMed: 25369000]
31. Shin J-H, Helmann JD. Molecular logic of the Zur-regulated zinc deprivation response in *Bacillus subtilis*. Nat Commun. 2016; 7
32. Ma Z, Gabriel SE, Helmann JD. Sequential binding and sensing of Zn(II) by *Bacillus subtilis* Zur. Nucleic Acids Res. 2011; 39:9130–9138. [PubMed: 21821657]
33. Natori Y, et al. A fail-safe system for the ribosome under zinc-limiting conditions in *Bacillus subtilis*. Mol Microbiol. 2007; 63:294–307. [PubMed: 17163968]
34. Dalecki AG, Crawford CL, Wolschendorf F. Copper and Antibiotics: Discovery, Modes of Action, and Opportunities for Medicinal Applications. Adv Microb Physiol. 2017; 70:193–260. [PubMed: 28528648]
35. Foster AW, Osman D, Robinson NJ. Metal preferences and metallation. J Biol Chem. 2014; 289:28095–28103. [PubMed: 25160626]
36. Warren MJ, Raux E, Schubert HL, Escalante-Semerena JC. The biosynthesis of adenosylcobalamin (vitamin B12). Nat Prod Rep. 2002; 19:390–412. [PubMed: 12195810]
37. Frank S, et al. Anaerobic synthesis of vitamin B12: characterization of the early steps in the pathway. Biochem Soc Trans. 2005; 33:811–814. [PubMed: 16042604]
38. Raux E, Thermes C, Heathcote P, Rambach A, Warren MJ. A role for *Salmonella typhimurium cbiK* in cobalamin (vitamin B12) and siroheme biosynthesis. J Bacteriol. 1997; 179:3202–3212. [PubMed: 9150215]
39. Lobo SA, et al. Two distinct roles for two functional cobaltochelatases (CbiK) in *Desulfovibrio vulgaris* hildenborough. Biochemistry. 2008; 47:5851–5857. [PubMed: 18457416]
40. Martin JE, Lisher JP, Winkler ME, Giedroc DP. Perturbation of manganese metabolism disrupts cell division in *Streptococcus pneumoniae*. Mol Microbiol. 2017; 104:334–348. [PubMed: 28127804]
41. Brown DR, et al. The cellular prion protein binds copper *in vivo*. Nature. 1997; 390:684–687. [PubMed: 9414160]
42. Bush AI. The metallobiology of Alzheimer's disease. Trends Neurosci. 2003; 26:207–214. [PubMed: 12689772]
43. McCarthy RC, Kosman DJ. Iron transport across the blood–brain barrier: development, neurovascular regulation and cerebral amyloid angiopathy. Cell Mol Life Sci. 2015; 72:709–727. [PubMed: 25355056]
44. Xiao T, et al. Copper regulates rest-activity cycles through the locus coeruleus-norepinephrine system. Nat Chem Biol. 2018; 14:655–663. [PubMed: 29867144]
45. Hood MI, Skaar EP. Nutritional immunity: transition metals at the pathogen–host interface. Nat Rev Microbiol. 2012; 10:525–537. [PubMed: 22796883]
46. Lisher JP, Giedroc DP. Manganese acquisition and homeostasis at the host-pathogen interface. Front Cell Infect Microbiol. 2013; 3:91. [PubMed: 24367765]
47. Wilks A, Burkhard KA. Heme and virulence: how bacterial pathogens regulate, transport and utilize heme. Nat Prod Rep. 2007; 24:511–522. [PubMed: 17534527]
48. Djoko KY, Ong C-lY, Walker MJ, McEwan AG. The role of copper and zinc toxicity in innate immune defense against bacterial pathogens. J Biol Chem. 2015; 290:18954–18961. [PubMed: 26055706]

49. Damo SM, et al. Molecular basis for manganese sequestration by calprotectin and roles in the innate immune response to invading bacterial pathogens. Proc Natl Acad Sci USA. 2013; 110:3841–3846. [PubMed: 23431180]
50. Lemire JA, Harrison JJ, Turner RJ. Antimicrobial activity of metals: mechanisms, molecular targets and applications. Nat Rev Microbiol. 2013; 11:371–384. [PubMed: 23669886]
51. Chivers PT, Benanti EL, Heil-Chapdelaine V, Iwig JS, Rowe JL. Identification of Ni-(L-His)$_2$ as a substrate for NikABCDE-dependent nickel uptake in *Escherichia coli*. Metallomics. 2012; 4:1043–1050. [PubMed: 22885853]
52. Livak KJ, Schmittgen TD. Analysis of relative gene expression data using real-time quantitative PCR and the $2^{-\Delta\Delta CT}$ method. Methods. 2001; 25:402–408. [PubMed: 11846609]
53. Ramakers C, Ruijter JM, Deprez RHL, Moorman AFM. Assumption-free analysis of quantitative real-time polymerase chain reaction (PCR) data. Neurosci Lett. 2003; 339:62–66. [PubMed: 12618301]
54. Chivers PT, Sauer RT. NikR repressor: high-affinity nickel binding to the C-terminal domain regulates binding to operator DNA. Chem Biol. 2002; 9:1141–1148. [PubMed: 12401498]
55. Romao CV, et al. Evolution in a family of chelatases facilitated by the introduction of active site asymmetry and protein oligomerization. Proc Natl Acad Sci U S A. 2011; 108:97–102. [PubMed: 21173279]
56. Stookey LL. Ferrozine-a new spectrophotometric reagent for iron. Anal Chem. 1970; 42:779–781.
57. Dainty SJ, Patterson CJ, Waldron KJ, Robinson NJ. Interaction between cyanobacterial copper chaperone Atx1 and zinc homeostasis. J Biol Inorg Chem. 2010; 15:77. [PubMed: 19543924]
58. Kuzmic P. Program DYNAFIT for the analysis of enzyme kinetic data: application to HIV proteinase. Anal Biochem. 1996; 237:260–273. [PubMed: 8660575]
59. Reyes-Caballero H, Lee CW, Giedroc DP. *Mycobacterium tuberculosis* NmtR harbors a nickel sensing site with parallels to *Escherichia coli* RcnR. Biochemistry. 2011; 50:7941–7952. [PubMed: 21819125]
60. Xiao Z, et al. Unification of the copper(I) binding affinities of the metallo-chaperones Atx1, Atox1, and related proteins: detection probes and affinity standards. J Biol Chem. 2011; 286:11047–11055. [PubMed: 21258123]

Europe PMC Funders Author Manuscripts

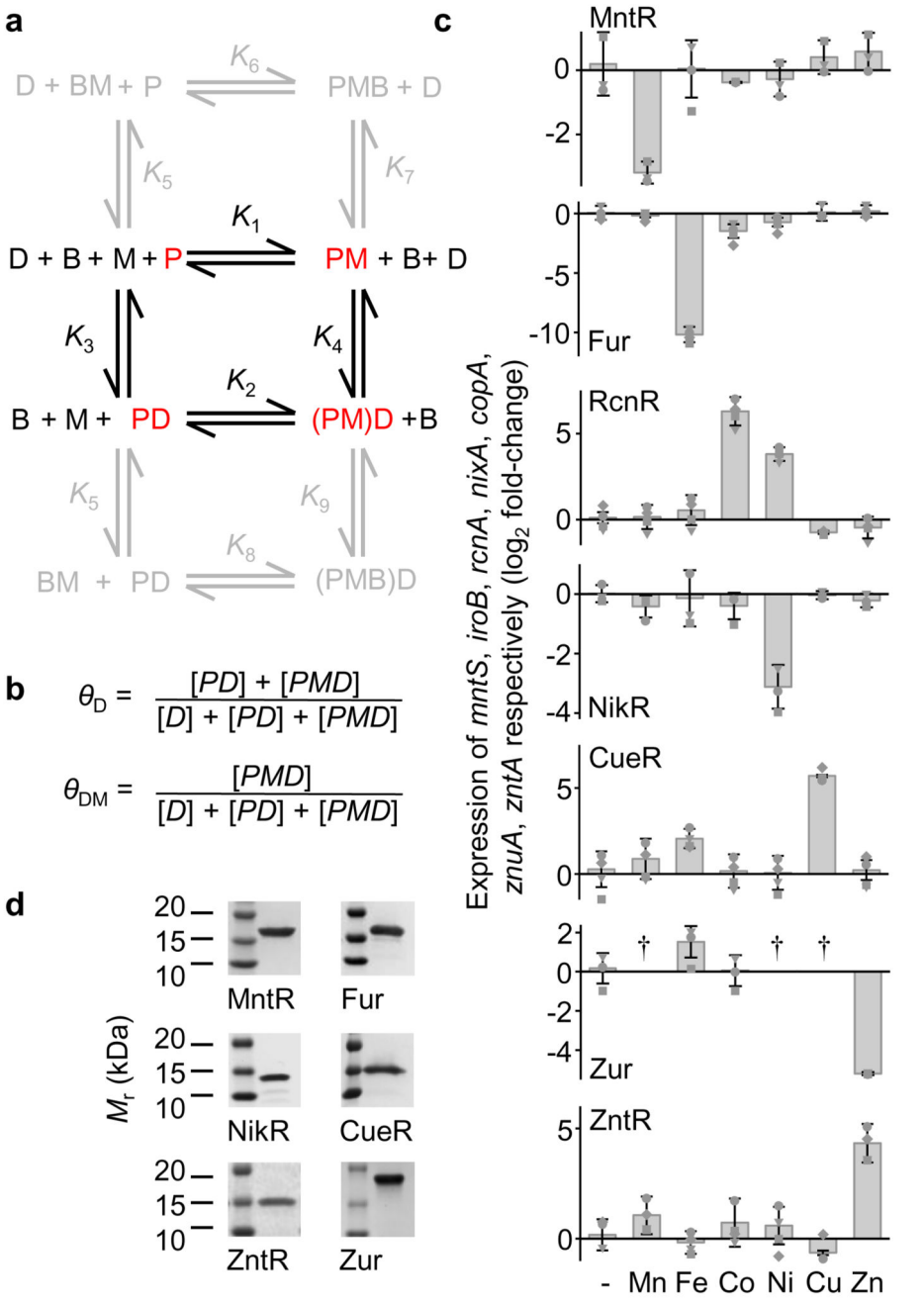

Figure 1. Metal binding and DNA binding are coupled to enable *Salmonella* to sense different metals.

a, Semi-schematic representation of metal sensors in four allosteric conformations (end states, red) which are thermodynamically coupled: apo (i.e. metal free)-protein (P), metal-protein (PM), apo-protein-DNA (PD) or metal-protein-DNA ((PM)D)7. Buffered metals (BM) may exchange to and from proteins via association of the molecules. **b**, The fractions of DNA target sites bound to sensor protein (θ_D) or solely to metalated sensor protein (θ_{DM}). **c**, qPCR ($\log_2$ fold-change) of *mntS* (regulated by MntR), *iroB* (regulated by Fur),

rcnA (regulated by RcnR), *nixA* (regulated by NikR), *copA* (regulated by CueR), *znuA* (regulated by Zur) and *zntA* (regulated by ZntR) in cells grown in elevated non-lethal metal concentrations. Data are the mean ± standard deviation (s.d.) of biologically independent samples (n = 4 for *iroB*, *rcnA*, *copA*, *zntA*; n = 3 for *mntS*, *nixA*, *znuA*; †, not analysed). Symbol shapes represent individual experiments. **d**, Purified sensor proteins analysed by SDS-PAGE (full images in Supplementary Fig. 3b). Using gradient SDS-PAGE, n = 1.

Europe PMC Funders Author Manuscripts

Europe PMC Funders Author Manuscripts

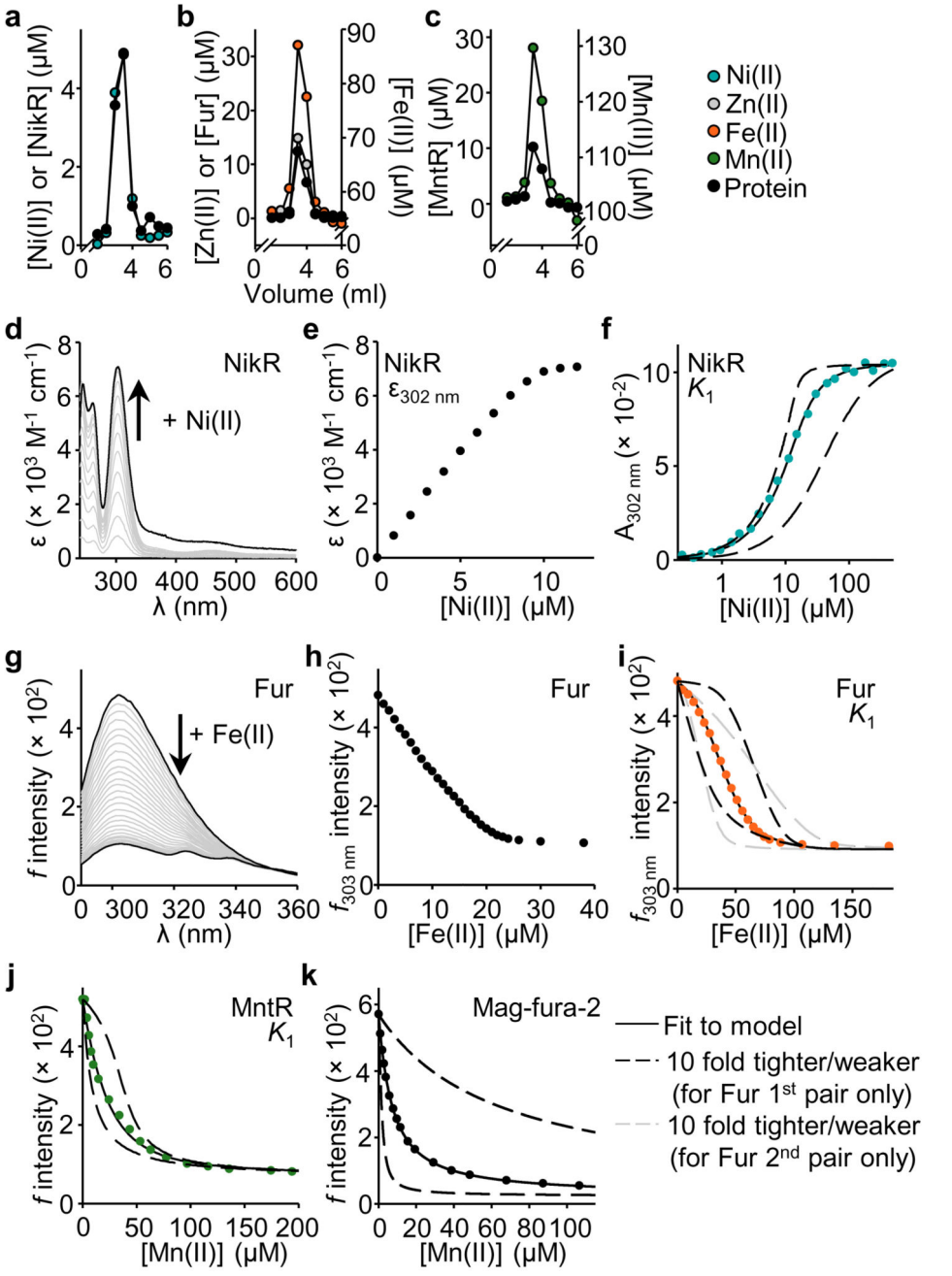

Figure 2. Metal affinities that complete a set of values for *Salmonella* metal sensors.

a-c, Gel-filtration (Supplementary Fig. 3c in full) showing co-migration of NikR with Ni(II) (**a**), Fur with Fe(II) and Zn(II) (**b** and Supplementary Fig. 4), MntR with Mn(II) (**c**). n = 1 (**a-c**). **d**, Apo-subtracted spectra of Ni(II)-titrated NikR (10.6 μM), n = 1 at pH 8.0. **e**, Feature at 302 nm from **d**, showing linear increase saturating at ~ 10 μM Ni(II), hence 1:1 Ni(II):NikR stoichiometry. **f**, Representative NikR (13.2 μM) absorbance (n = 4 independent experiments) in competition for Ni(II) with EGTA (784.3 μM). The fit departs from simulations with K_{Ni} ten-fold tighter or weaker. **g**, Quenching of Fur (10.3 μM) fluorescence

emission by Fe(II). n = 3 independent experiments with similar results. **h**, Feature at 303 nm from **g**. **i**, Representative Fur (10.2 μM) fluorescence in competition for Fe(II) with NTA (100 μM) (n = 4 independent experiments). The fit departs from simulations with K_{Fe} ten-fold tighter or weaker for the first pair (second pair K_{Fe} fixed) and second pair (first pair K_{Fe} fixed) of sites. **j**, Representative mag-fura-2 (1.95 μM) fluorescence (n = 4 independent experiments) in competition for Mn(II) with MntR (18.7 μM). The fit departs from simulations with K_{Mn} for MntR ten-fold tighter or weaker. **k**, Mn(II) binding to mag-fura-2 from Supplementary Figure 5 (n = 4 independent experiments), 1:1, $\lambda_{excitation}$ 380 nm, with simulations ten-fold tighter and ten-fold weaker than the fitted mean (±s.d.) K_{Mn} of 6.1 (±0.4) × 10^{-6} M for mag-fura-2. Fitting models in Supplementary Note 1.

Europe PMC Funders Author Manuscripts

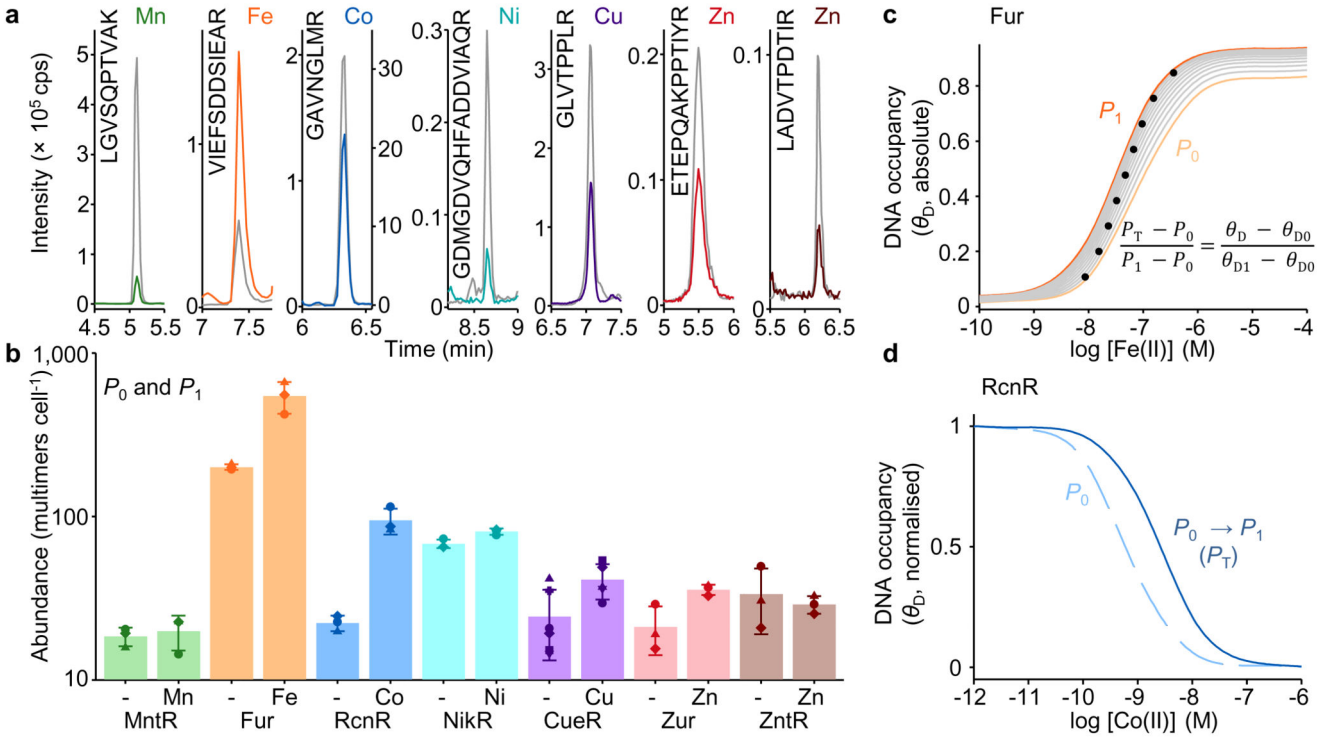

Figure 3. Metals change the abundance of some sensors to modify regulation.

a, Representative chromatograms following MRM mass-spectrometry of ion transitions for analyte (coloured lines) or isotope-labelled internal standards (grey line, right axis for RcnR) for MntR, Fur, RcnR, NikR, CueR, Zur and ZntR respectively, detected in *Salmonella* cell lysates following prolonged exposure to elevated concentrations of cognate metals (n = 3 biologically independent samples, other than CueR where n = 5 biologically independent samples, with similar results). Multimeric states are noted in Table 1 footnote. Analyte peptide sequence is shown for each protein. Full chromatograms shown in Supplementary Figure 9. **b**, Abundance of sensors in control cells in minimal media P_0 (left) and with cognate metal P_1 (right). Values were calculated using calibration curves (Supplementary Fig. 8a) normalised to cell number. Bars and error bars are means and s.d., respectively (shapes represent biologically independent experiments with n = 3, except for CueR where n = 6 (P_0) and n = 5 (P_1)). **c**, Fractional DNA occupancy (θ_D) with Fur as a function of buffered [Fe(II)] using K_1, K_3, K_4, target DNA concentration (Table 1), and either P_0 (light orange line), P_1 (dark orange line) or 10% increments between P_0 and P_1 (grey lines). DNA occupancy (black circles) where [Fur] at any given [cognate metal] (P_T) is linearly proportional to θ_D (inset). θ_{D0} and θ_{D1} (determined using P_0 and P_1), are DNA occupancies at low and high [cognate metal], respectively. For co-repressors (e.g. Fur), θ_{D0} and θ_{D1} are minimum and maximum values (the converse relationship for de-repressors). **d**, A comparison of θ_D with RcnR using P_T (solid blue line) relative to fixed [RcnR] and P_0 (dashed light blue), normalised independently for each curve.

Europe PMC Funders Author Manuscripts

Europe PMC Funders Author Manuscripts

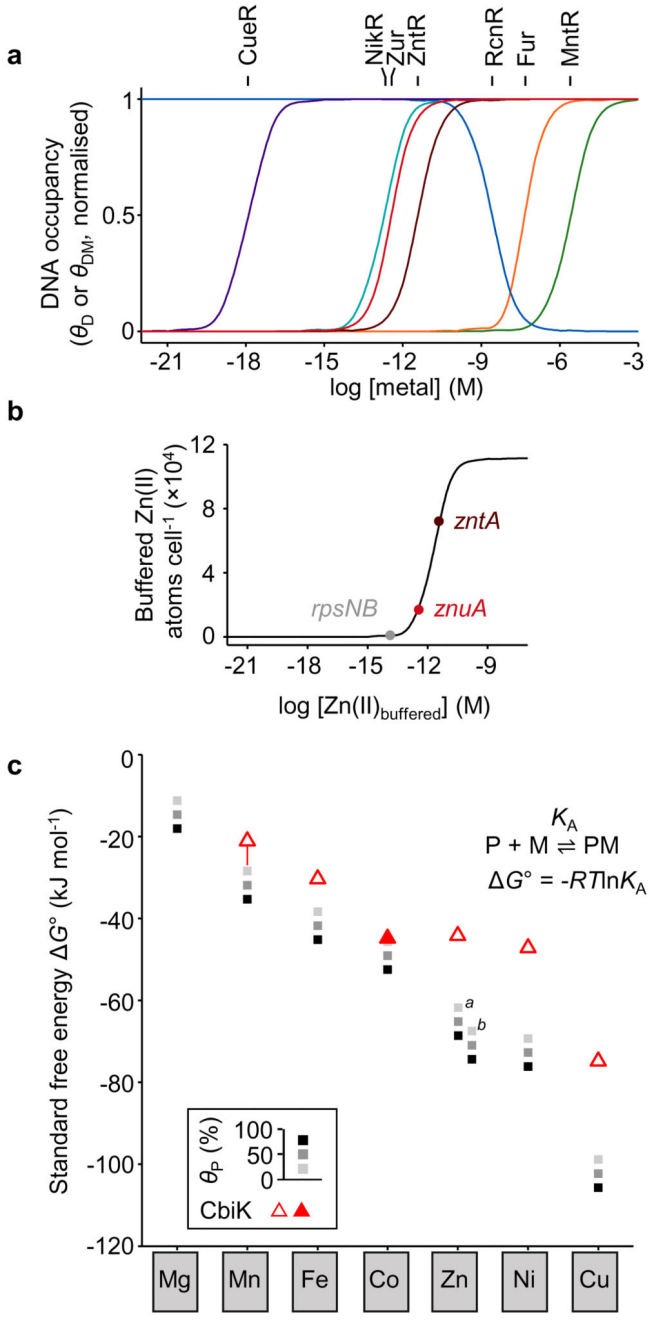

Figure 4. Sensing is tuned to the Irving-Williams series.

a, Calculated responses of CueR, NikR, Zur, ZntR, RcnR, Fur and MntR, as θ_D (or θ_{DM} for ZntR and CueR), to buffered concentrations of Cu(I), Ni(II), Zn(II), Zn(II), Co(II), Fe(II) and Mn(II) respectively within *Salmonella* using metal affinities, DNA affinities, cellular protein and DNA target abundances, in Table 1, Supplementary Figure 8 and Supplementary Table 1. **b**, Relationship between buffered Zn(II) concentration and total Zn(II) ions in a simulated buffer, showing where *Salmonella* Zur and ZntR, plus *B. subtilis* Zur on the *rpsN* promoter (Supplementary Fig. 14), are calculated to undergo 0.5 of their responses. **c**,

Standard free energy change (ΔG°) for formation of a protein-metal (PM) complex, which in the *Salmonella* cytosol, corresponds to 20%, 50% or 80% metalation (θ_P): Zn(II) determined for ZntR (*a*), and Zur (*b*); riboswitch used for Mg(II) (Supplementary Table 2). Triangles, ΔG° for CbiK. For Mn(II), the arrow represents a limiting affinity of 20 μM or less.

Europe PMC Funders Author Manuscripts

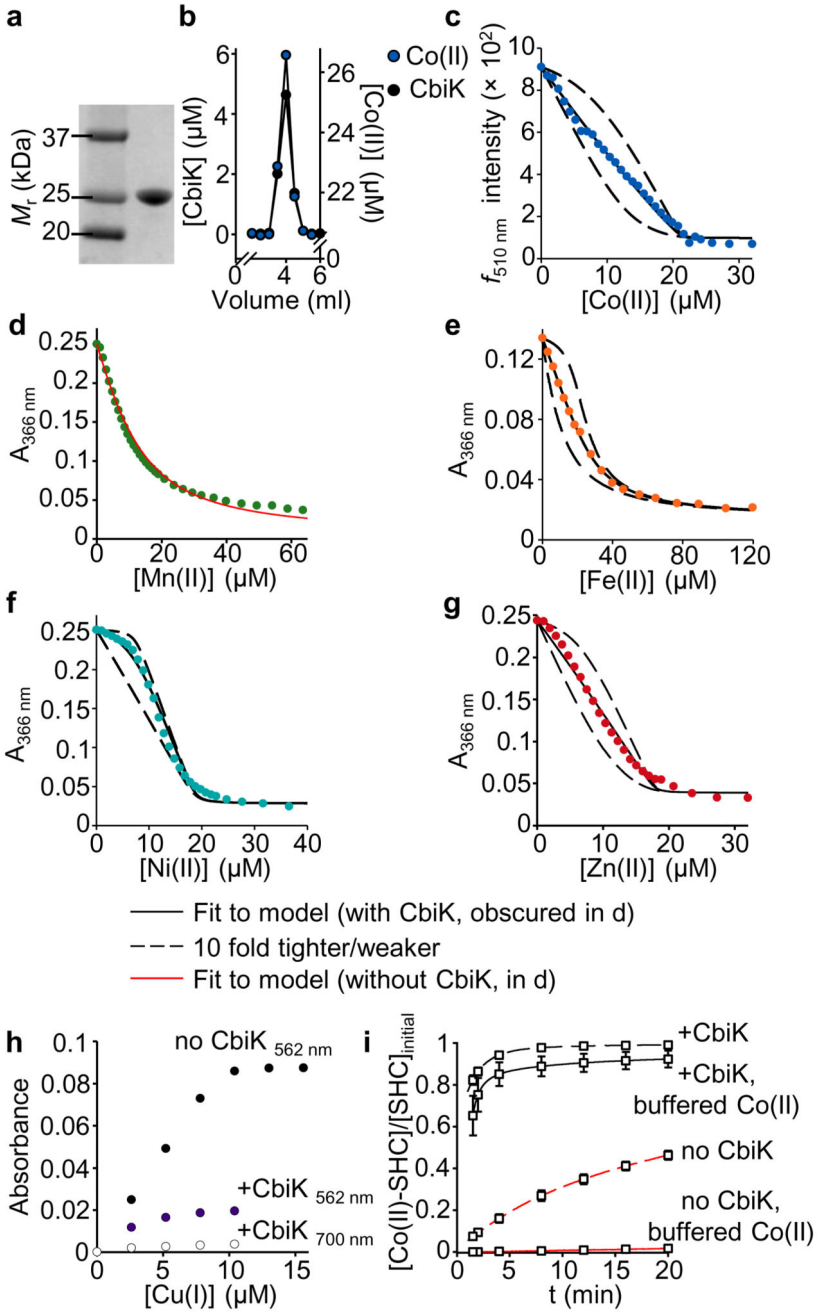

Figure 5. Metalation of CbiK and sirohydrochlorin.

a, SDS-PAGE of CbiK (Supplementary Fig. 16a). n = 1 by gradient SDS-PAGE. **b**, Gel-filtration of CbiK in 20 μM Co(II) (Supplementary Fig. 16b) (n = 3 independent experiments with similar results). **c**, Fura-2 (12.6 μM) fluorescence (n = 3 independent experiments) competing for Co(II) with CbiK (8.59 μM). **d**, Mag-fura-2 (11.3 μM) absorbance (n = 3 independent experiments) outcompeting CbiK for Mn(II) (7.38 μM): Fits with and without CbiK overlay. **e**, Mag-fura-2 (6.08 μM) absorbance (n = 3 independent experiments) competing for Fe(II) with CbiK (19 μM). **f**, Mag-fura-2 (11.3 μM) absorbance (n = 3

independent experiments) competing for Ni(II) with CbiK (7.46 μM). **g**, Mag-fura-2 (11 μM) absorbance (n = 3 independent experiments) competing for Zn(II) with CbiK (6.84 μM). In **c**, **e**–**g**, fits depart from K_{metal} ten-fold tighter or weaker noting that Ni(II) approaches the tightest limit for the assay. All models in Supplementary Note 1. **h**, BCA (22.1 μM) absorbance without (n = 3 independent experiments) or with (n = 4 independent experiments) competition for Cu(I) with CbiK (10 μM). Representative data sets are shown in **c**–**h**. **i**, Conversion of sirohydrochlorin (4.67-5.64 μM) after addition of Co(II) with or without CbiK (5 μM), plus or minus a Co(II)-buffer (data are means of n = 3 independent experiments ±s.d.). Full time course shown in Supplementary Figure 22.

Europe PMC Funders Author Manuscripts

Table 1

Metal affinities, DNA affinities, allosteric coupling free energies and DNA targets of *Salmonella* metal sensors

Sensor/ Metal	K_{Metal} ($1/K_1$) (M)*	K_{DNA} ($1/K_3$) (M) (without metal)	K_{DNA} ($1/K_4$) (M) (with metal)	ΔG_C (kcal mol^{-1})	No. DNA targets†
MntR/ Mn(II)	1.3 (±0.4) × 10^{-5}	8.6 (±1.7) × 10^{-8}	5 × 10^{-9}§§	-1.7 (±0.1)	4
Fur/ Fe(II)	5.3 (±0.7) × 10^{-7}‡	2.4 (±0.6) × 10^{-5}	5.6 (±2.1) × 10^{-8}	-3.6 (±0.2)	37
RcnR/ Co(II)	5.1 (±0.9) × 10^{-10}‡‡	1.5 (±0.8) × 10^{-7}‡‡	1.5 (±0.2) × 10^{-5}‡‡	+2.7 (±0.2)‡‡	1
NikR/ Ni(II)	2.5 (±0.4) × 10^{-12}	1.1 (±0.1) × 10^{-5}	9.5 (±0.8) × 10^{-9}	-4.2 (±0.1)	2
CueR/ Cu(I)	3.3 (±0.7) × 10^{-19}‡‡	3.2 (±1.2) × 10^{-8}§	3.8 (±1.8) × 10^{-7}§	+1.4 (±0.4)§	3
Zur/ Zn(II)	6.4 (±0.4) × 10^{-13}‡‡	2.7 (±0.4) × 10^{-5}‡‡	4.1 (±1.0) × 10^{-8}‡‡	-3.9 (±0.2)‡‡	4
ZntR/ Zn(II)	3.2 (±0.7) × 10^{-12}‡‡	1.1 (±0.4) × 10^{-7}	7.8 (±1.3) × 10^{-7}	+1.2 (±0.2)	1

All constants are means ± s.d., with 'n' of independent replicates stated in the legends of Figure 2 and Supplementary Figure 6 (other than values marked ‡‡, see below), and are presented here as dissociation constants. ΔG_C is the free energy coupling metal binding to DNA binding.

*Metal-binding data were fit to models describing a single affinity for the complement of allosterically effective site(s) of each sensor: This is an apparent average affinity of four sites per MntR dimer, two per Fur or Zur dimer, two per RcnR tetramer, four per NikR tetramer, and one per CueR or ZntR dimer. It is noted that two sites appear sufficient for allosteric regulation by MntR on some promoters, and Supplementary Figure 14 examines an analogous situation for some Zur-regulated promoters.

†The identified DNA binding sites for each sensor are listed in Supplementary Table 1.

‡For Fur, to fit the data in Figure 2i, it was necessary to consider sequential Fe(II) binding events to four sites per Fur dimer, with individual (mean (±s.d.)) affinities $1/K_1$ of 2.6 (±0.3) × 10^{-7} M for the two allosteric sites which was converted to a single value describing the filling of both sites. The individual (mean (±s.d.)) affinities $1/K_1$ of sites three and four was 6.4 (±0.6) × 10^{-8} M.

‡‡Determined previously11,23, limiting values confirmed by low-salt titrations, Supplementary Figure 11 for Zur.

§Values are for DNA binding by the first CueR dimer. Mean (±s.d.) DNA affinities $1/K_3$ and $1/K_4$ of the second dimer binding were 1.0 (±0.4) × 10^{-6} M and 3.9 (±1.7) × 10^{-8} M for apo- and Cu(I)-CueR, respectively.

§§Confirmed by titration with 2 nM DNA (n = 6 independent experiments).